

Orbital Selective Kondo Effect in Heavy Fermion Superconductor UTe_2

Byungkyun Kang,^{1,2,*} Sangkook Choi,² and Hyunsoo Kim^{3,†}

¹*Department of Physics and Astronomy, University of Nevada, Las Vegas, Nevada 89154, USA*

²*Condensed Matter Physics and Materials Science Department,
Brookhaven National Laboratory, Upton, NY 11973, USA*

³*Department of Physics and Astronomy, Texas Tech University, Lubbock, Texas 79409-1051, USA*

(Dated: November 18, 2021)

The electronic structure of heavy fermion superconductor UTe_2 is calculated by means of *ab initio* linearized quasiparticle self-consistent GW and dynamical mean field theory. We demonstrate that the recent experimental observations associated with the Kondo effect can be sufficiently explained when the spin-orbit coupling (SOC) is included. SOC triggers the single-ion Kondo scattering around 500 K, and the scattering process undergoes incoherent-to-coherent crossover around 50 K upon cooling, evidenced by the appearance of a coherent peak at the Fermi level. We found that the hybridization between U-5*f* and U-6*d* predominantly in the orthorhombic *ab*-plane is responsible for the high-temperature Kondo effect. This result is consistent with the negative slope near room temperature followed by the drastic downturn around 50 K observed in the in-plane resistivity. In contrast, the hybridization between U-5*f* and Te-5*p* along the *c*-axis manifests the Kondo scattering at a much lower temperature of ~ 50 K, which could be responsible for the low-temperature upturn of the *c*-axis resistivity. Our results suggest that the Kondo effect in UTe_2 is highly orbital selective, which naturally elucidates the anomalous temperature dependence of resistivity reported by Y. S. Eo et al. [1].

Introduction - The uranium-based superconductors are promising candidates for the realization of the spin-triplet superconductivity [2]. The prominent examples include URhGe [3] and UCoGe [4] with the critical temperature $T_c = 0.25$ K and 0.8 K, respectively. Both compounds undergo the superconducting phase transition from the ferromagnetically ordered state, making the equal spin pairing plausible [2]. Recently, superconductivity was discovered in *Curie paramagnetic* UTe_2 with $T_c \approx 2$ K [5–7] that is one of the highest among the known uranium-based superconductors. T_c can be further enhanced nearly two-fold at approximately 1 GPa [8, 9]. However, the mechanism behind this celebrated high T_c has not been resolved. The main obstacle is insufficient knowledge of the electronic structure of the normal state in UTe_2 , which is a prerequisite for the understanding of superconductivity.

UTe_2 exhibits the iconic incoherent-to-coherent crossover around $T = 50$ K in the resistivity with an electrical current along the orthorhombic *a*-direction [5, 10], which is reminiscent of prototypical Kondo lattice YbRh_2Si_2 [11]. Both UTe_2 and YbRh_2Si_2 exhibit a negative slope in electrical resistivity at room temperature, implying that inelastic scattering dominates over the electron-phonon scattering. The magnetic contribution of resistivity is suggestive of $-\ln T$ dependence observed in most of the Kondo lattice systems above the coherent temperature T^* , for instance, in-plane resistivity in CeCoIn_5 between $T = 40$ K and 180 K [12]. While the Kondo scattering is not the only possibility for the resistivity upturn, recent spectroscopy experiments successfully observed the formation of a hybridized band well above the coherent temperature in CeCoIn_5 [13, 14]. Most notably a combined study of ARPES and DMFT identified the occurrence of Kondo resonance up to 200 K in CeCoIn_5 [15]. In contrast, no hybridization gap has been observed in UTe_2 at any temperature, leaving the scattering mechanism in the normal state elusive in

this new heavy-fermion compound.

The *c*-axis transport property in UTe_2 is qualitatively different where it is metallic between 50 K and at least 300 K. The *c*-axis resistivity shows a rapid upturn below 50 K before exhibiting coherent-like behavior at the onset around 13 K [1]. Moreover, magnetic susceptibility below ~ 100 K shows distinct temperature-dependence in all three symmetry directions [5, 10]. The anisotropic transport and magnetic properties suggest that the orbital-dependent electron correlation needs to be taken into account. These outstanding issues put heavy-fermion UTe_2 in a league of its own, and thus the understanding of the electronic structure of its normal state is the most pressing issue. While several ARPES studies were reported [16, 17], a complete picture of the band structure is still awaited. Therefore, theoretical determination of the accurate band structure is highly desired.

The normal state of UTe_2 can be best explained within a framework of Kondo lattice where the periodic local magnetic moments are screened by spins of conduction electrons [18]. The Ce-based Kondo lattice has been most widely studied by the dynamical mean field theory combined with density functional theory (DFT+DMFT) [15, 19–23]. In a recent study by Choi et al. [19], the temperature evolution of the Kondo effect was illustrated by analyzing the spectral function $A(\mathbf{k}, \omega)$ for CeCoGe_2 . The incoherent Ce-4*f* state is hybridized with conduction electrons (*f*-*c* hybridization), and the stronger contribution of Ce-4*f* state near the Fermi level distorts conduction electron bands, resulting in kinks in the bands at the Fermi level. At low temperatures, the incoherent Ce-4*f* state forms coherent bands with the renormalized carriers, initiating the coherent Kondo lattice states. The *f*-*c* hybridization, which is an indispensable element in Kondo physics, occurs selectively in the type of orbitals. In CeCoIn_5 , the selective *f*-*c* hybridization of two *d* bands and three crystalline electric-field split *f* levels gives rise to different dispersion of *d* bands in

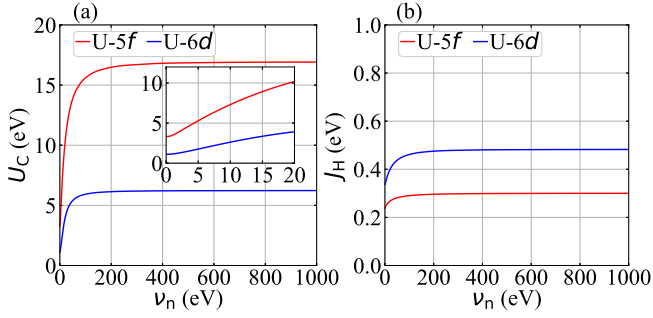


FIG. 1. Calculated (a) U_C for U-5f and U-6d, and (b) J_H for U-5f and U-6d in UTe₂ with inclusion of SOC. Insets in (a) shows magnified views of U_C in low frequency range.

the vicinity of the Fermi level [15]. In PuCoGa₅, the Fermi-liquid behavior appears differently depending on Pu-5f states in $j = 5/2$ or $j = 7/2$ multiplet, which are induced by spin-orbit coupling (SOC), resulting in larger Kondo scale for f electrons in $j = 5/2$ than $j = 7/2$ multiplet [24].

The role of SOC in the Kondo effect is a long standing issue [25], for which UTe₂, comprising heavy elements, is a new avenue. Obviously, SOC has a significant influence on the band structure in UTe₂ as well as its superconductivity. To date, there are two DFT+DMFT studies on UTe₂ without considering SOC [17, 26]. Both show a flat peak hybridized with conduction electrons at 10 K and the peak was suppressed at 200 K, suggesting Kondo coherence at low temperature.

In this work, we ascertain the electronic structure of UTe₂ without adjusting parameters and its temperature evolution with/without the inclusion of SOC. By inclusion of SOC, we found a multi-scaled Kondo effect. The SOC causes degenerated U-5f states of the non-SOC system to split into partially occupied states in $j = 5/2$ and unoccupied states in $j = 7/2$ multiplet. Within the $j = 5/2$ subspace, we found two groups of U-5f states, which selectively hybridize with conduction electrons p or d , giving rise to the orbital-dependent Kondo effect.

Methods - We use *ab initio* linearized quasiparticle self-consistent GW (LQSGW) and dynamical mean field theory (DMFT) method [27–29] to calculate the electronic structure of UTe₂ which crystallizes into orthorhombic space group Immm (No. 71) [30, 31]. The LQSGW+DMFT is designed as a simplified version of the full GW+EDMFT approach [32–34]. It calculates electronic structure by using LQSGW approaches [35, 36]. Then, it corrects the local part of GW self-energy within DMFT [37–39]. Within the methodology, the only parameters we adopted from experiments are lattice constants ($a = 4.1611$, $b = 6.1222$, $c = 13.955$ Å) [31], and we explicitly calculate all other quantities such as double-counting energy and Coulomb interaction tensor. Then, local self-energies for U-5f and U-6d are obtained by solving two different single impurity models. For the details, please see the supplemental materials.

Coulomb interaction tensor and electron occupation - First,

we calculate onsite Coulomb interaction U_C and exchange interaction J_H within the constrained random phase approximation (cRPA) [40, 41]. The calculated U_C and J_H for both U-5f and U-6d orbitals with inclusion of SOC are shown in Fig. 1 (see Fig. S1 for non-SOC result). Both U_C and J_H increase and saturate to the bare unscreened value at high frequency.

Using the Coulomb interaction tensor, the electron occupancy of U-5f orbitals at 300 K are subsequently calculated including SOC, which is presented in Table I. The total occupation in U-5f orbitals is 2.27. The SOC split U-5f into $j = 5/2$ and $j = 7/2$ multiplet, resulting in pushing U-5f states of non-SOC system, which are centered around 0.3 eV above the Fermi level (see Fig. 2 (d)). This interaction gives rise to partially occupied $j = 5/2$ states and unoccupied $j = 7/2$ states. On the contrary, the U atom is strongly oxidized in the non-SOC simulation where the corresponding electron is transferred to Te-5p orbitals, and the resultant occupancy is 1.17 which is significantly smaller than that from the SOC simulation. The occupation numbers exhibit no sizeable temperature variation from 25 K to 2000 K. The calculated U-5f occupation with SOC is in good agreement with the measured $5f^2$ configuration [42].

Kondo Scattering driven by SOC - To learn the Kondo effect due to the localized U-5f in UTe₂, we calculated the spectral function at various temperatures along the high symmetry orientations depicted in Fig. 2 (a). The calculated spectral functions with and without SOC at 300 K are respectively shown in Fig. 2 (b) and (c). Within SOC simulation, the flat heavy electron and hole bands are formed in the vicinity of the Fermi level along every high symmetry line. (see also Fig. 3 (a)). Within the non-SOC simulation, the coherent bands near the Fermi energy are comprised of U-5f, U-6d, and Te-5p orbitals, and the flat bands do not form down to 100 K.

Figures 2 (d) and (e) show the projected DOSs for U-5f and U-6d orbitals, respectively. The results with and without SOC are shown in red and blue lines, respectively. In the SOC system, a sharp U-5f peak emerges about 0.02 eV above the Fermi level, whereas a sharp U-5f peak is centered around 0.3 eV above the Fermi level in the non-SOC system. In comparison to U-5f occupation of 1.17 in the non-SOC system, the SOC system manifests a higher U-5f occupation of 2.27 in the larger U-5f DOS below the Fermi level (see inset of Fig. 2(d)). In the non-SOC system, three coherent peaks appear between -1 eV and 0 eV, which are hybridized with U-6d as shown in Fig. 2 (e). In contrast, the U-5f and U-6d DOSs below the Fermi level are broad in the SOC system, and the shape of the U-5f spectral function is consistent with incoherent states.

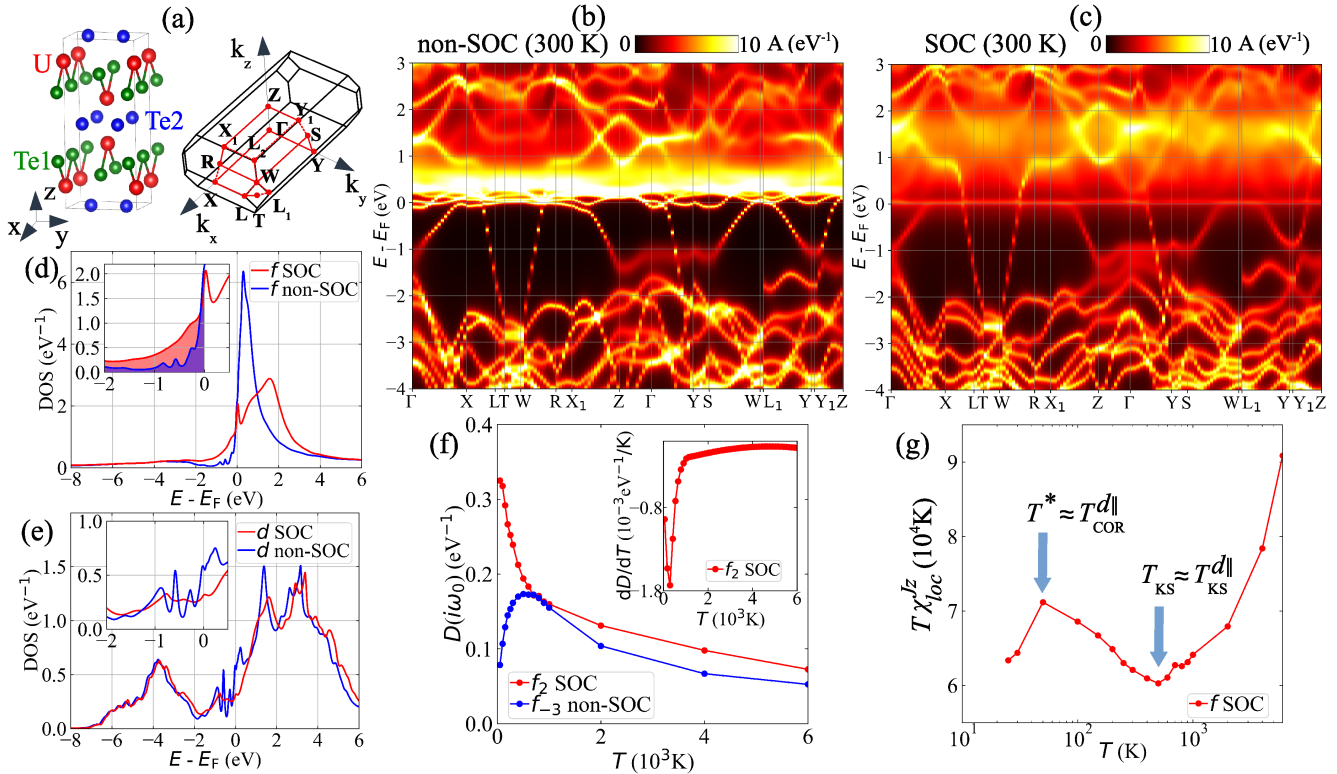
Figure 2 (f) shows the temperature dependence of U-5f projected DOS at the Fermi level, which is determined by

$$D(i\omega_0) = -\frac{1}{\pi} \text{Im}G(i\omega_0) \quad (1)$$

where ω_0 is the first Matsubara frequency and G is the calculated local Green's function. $D(i\omega_0)$ for both SOC f_2 and

TABLE I. Calculated electron occupation of U-5*f* orbitals in UTe₂ at $T = 300$ K. U-5*f* orbitals are labelled for convenience in this work.

j	5/2						7/2							
j_z	-2.5	-1.5	-0.5	0.5	1.5	2.5	-3.5	-2.5	-1.5	-0.5	0.5	1.5	2.5	3.5
occupation	0.39	0.22	0.39	0.40	0.22	0.42	0.02	0.03	0.03	0.03	0.03	0.03	0.03	0.02
label	f_1	f_2	f_3	f_4	f_5	f_6	f_7	f_8	f_9	f_{10}	f_{11}	f_{12}	f_{13}	f_{14}


 FIG. 2. (a) Crystal structure and first Brillouin zone of UTe₂. (b) and (c) Calculated spectral function without and with inclusion of SOC at 300 K. (d) and (e) U-5*f* and U-6*d* projected DOSs with and without inclusion of SOC at 300 K. Insets show magnified views near the Fermi level. (f) f_2 and f_{-3} projected DOS at the Fermi level for SOC and non-SOC, respectively. Inset shows temperature derivation of f_2 DOS. (g) $T\chi_{loc}^{Jz}$ for U-5*f* with inclusion of SOC. The blue arrows point local minimum and maxima at which scales of Kondo effect were evaluated.

non-SOC f_{-3} ($l = 3, m = -3$) gradually increase upon cooling down to 700 K because of formation of quasiparticle peak where the spectral weight at the Fermi level is transferred from the upper and lower Hubbard bands [19, 43]. However, the SOC f_2 and non-SOC f_{-3} exhibit qualitatively different behavior below 700 K. Whereas $D(i\omega_0)$ of f_{-3} in the non-SOC system is rapidly reduced, that of f_2 in the SOC system soars. $\{f_1, f_3, f_4, f_5, f_6\}$ in $j = 5/2$ multiplet show the same temperature evolution with f_2 down to 300 K. We attribute the abruptly enhanced $D(i\omega_0)$ to the emergence of the Kondo scattering in the SOC system where abundant f DOS near the Fermi level facilitates the f - c hybridization. The six partially occupied U-5*f* orbitals in $j = 5/2$ multiplet are characterized with $-1/2$ spin by Hund's rule, and the total spin moment of the impurity increases, resulting in a relatively higher onset temperature of the Kondo screening process [44].

To investigate the relevant energy scales of Kondo physics,

we calculate the local total angular momentum susceptibility given as

$$\chi_{loc}^{Jz} = \int_0^\beta d\tau \langle J_z(\tau) J_z(0) \rangle. \quad (2)$$

Figure 2 (g) shows the product of temperature and χ_{loc}^{Jz} of U-5*f* as a function of temperature. The plot reveals two characteristic temperatures of Kondo lattice in UTe₂: Kondo scattering temperatures (T_{KS}) and lattice coherence temperature (T^*). The high temperature T_{KS} below which χ_{loc}^{Jz} deviates from the Curie-Weiss behaviors indicates the onset of the Kondo scattering process. The low temperature T^* with a local maximum of χ_{loc}^{Jz} suggests the crossover of incoherent-to-coherent scattering. Our estimation of $T^* \simeq 50$ K and $T_{KS} > 300$ K is consistent with the negative slope of ab -plane resistivity between 50 K and 300 K [1]. T_{KS} in UTe₂ is much

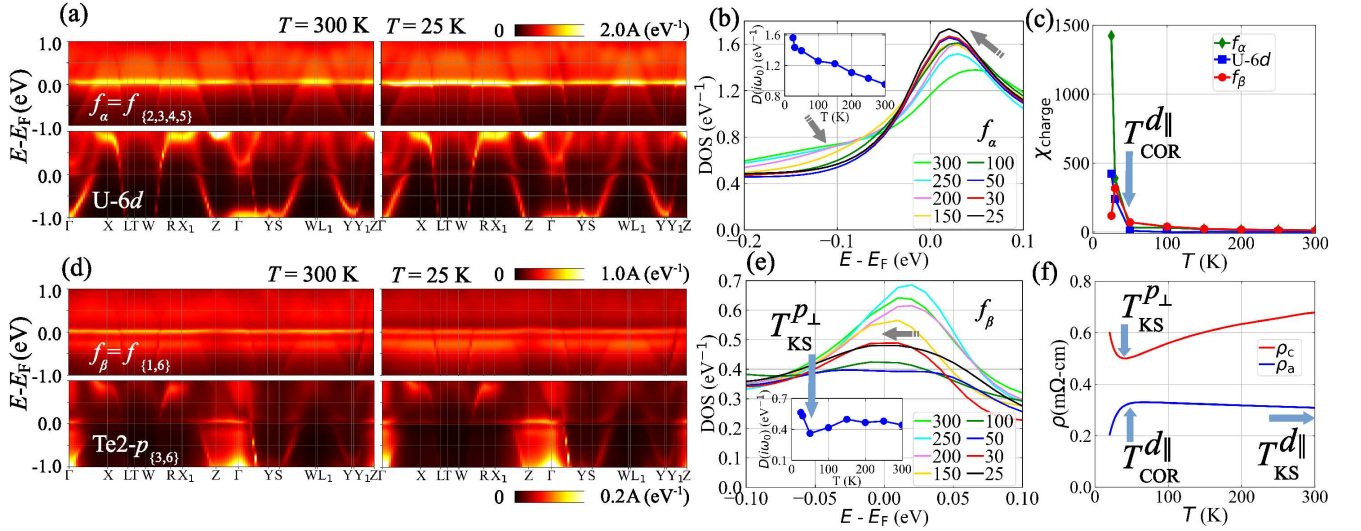


FIG. 3. (a) f_α and U-6d projected spectral functions at 300 (25) K in left (right) panel. (b) f_α projected DOS. The gray arrows denote peaks evolution at temperature lowering. Inset shows f_α DOS at the Fermi level. (c) Charge susceptibility of f_α , U-6d, and f_β orbitals. (d) f_β and Te2- $p_{\{3,6\}}$ projected spectral functions at 300 (25) K in left (right) panel. (e) f_β projected DOS. The gray arrow denotes the peak center is shifted below the Fermi level. Inset shows DOS at the Fermi level. (f) Corresponding scales of Kondo scattering are denoted on measured resistivity along the a and c axes. Note that the behavior of resistivity along the b axis (not shown here) is similar with ρ_a . In (b) and (e), the temperature unit is K.

higher than ~ 200 K in CeCoIn₅ [15] and CeCoGe₂ [19], and we attribute the higher T_{KS} to the larger total f valence electrons in U-5 f than Ce-4 f and strong SOC in UTe₂.

Orbital selective Kondo Scattering - To elucidate the transport properties in UTe₂ between $T = 25$ K and 300 K, we analyze the SOC system in depth. The crystal electric field and SOC lift the degeneracy of the U-5 f orbitals, grossly forming two groups, $f_\alpha = \{f_2, f_3, f_4, f_5\}$ and $f_\beta = \{f_1, f_6\}$ (see Table I), with an energy separation of ~ 0.12 eV. These two groups show distinct electronic structures in this temperature range in terms of DOS, spectral functions, and charge susceptibility. We found f_α and f_β are hybridized with U-6d and Te2- $p_{\{3,6\}}$ states, respectively. Here, Te2- $p_{\{3,6\}}$ includes Te2-5 p states of ($j = 3/2, j_z = -3/2$) and ($j = 3/2, j_z = 3/2$).

We computed orbital-resolved spectral functions, and the hybridization between f_α and U-6d is presented in Fig. 3 (a). The kink-like structure appears at the intersection of the two bands, which is consistent with the Kondo effect [19]. The abrupt change in the U-6d conduction bands dispersion at the Fermi level is clearly visible along the Γ -X, X₁-Z, S-W, and L₁-Y symmetry lines, all of which belong to the ab -plane. Thus, these hybridizations will affect electrical transport in the ab -plane. We define the onset temperature of Kondo scattering due to hybridization between f_α and U-6d, $T_{KS}^{d_{||}} \approx 500$ K at which the kink-like structure starts appearing at the Fermi level. Note that $T_{KS}^{d_{||}} \approx T_{KS}$, indicating f_α -orbitals are responsible for the high temperature Kondo effect. Below $T = 400$ K, the heavy mass dispersion appears, and the first excited state is disconnected, indicating the progression of the active Kondo scattering. At $T = 25$ K, the incoherent f_α -bands below the Fermi level are absent, and the coherent f_α peak above

the Fermi level is enhanced near the Fermi level, resulting in a single coherent peak (see Fig. 3 (a), (b), and Fig. S2). The formation of coherent f bands near the Fermi level signals renormalization of the carriers [19] and indicates the coherent Kondo lattice in UTe₂ [15]. We determine the crossover temperature $T_{cor}^{d_{||}}$ (often denoted by T^*) from the incoherent scattering to the coherent Kondo lattice by employing the charge susceptibility,

$$\chi_{\text{charge}} = \sum_i \int_0^\beta d\tau \langle n_i(\tau) n_i(0) \rangle - \beta \langle n_i \rangle^2 \quad (3)$$

where n_i is the occupation of i -th orbital, which evaluates charge fluctuation [45]. Figure 3 (c) shows the temperature dependent χ_{charge} of f_α (green) and U-6d (blue) which abruptly surge below $T_{cor}^{d_{||}} = 50$ K simultaneously. Our estimated $T_{KS}^{d_{||}} = 500$ K and $T_{cor}^{d_{||}} = 50$ K for the f_α and U-6d hybridization are in good agreement with experimental resistivity along the a - and b -axis, where ρ_a and ρ_b show $d\rho/dT < 0$ between 50 K and 300 K and start to drop rapidly around 50 K [1] as shown in Fig. 3 (f). Te1-5 p orbitals, hybridized with U-5 f and U-6d, constitute the conduction bands along the X-L, W-R, Γ -Y, and Y₁-Z symmetry lines. However, we did not find any evidence of the Kondo effect, and the hybridized bands remain metallic at high temperatures.

Below we focus on f_β -orbitals. Figure 3 (d) shows the f_β orbital-resolved spectral functions where f_β is hybridized with Te2- $p_{\{3,6\}}$ along Z- Γ in the vicinity of the Fermi level (see also Fig. S3 (a)). This result indicates that the conduction electron along the c -axis is originated from Te2- $p_{\{3,6\}}$.

The DOS of $\text{Te}2-p_{\{3,6\}}$ (data not shown) consists of spectral weight at the Fermi level over the entire temperature range and shows a small but notable increase as lowering the temperature. Figure 3 (e) shows f_β -projected DOS where a single coherent peak is present slightly above the Fermi level at high temperatures. The peak position approaches the Fermi level upon cooling, accompanied by a gradual reduction of the peak height. At $T = 50$ K, another peak appears below the Fermi level. The two peaks merge at $T < 50$ K, forming a single, enhanced peak at the Fermi level (see also Fig. S2). The temperature evolution of DOS of f_β at the Fermi level can shed light on the transport properties, and the inset of Fig. 3 (e) shows temperature evolution of $D(i\omega_0)$ of f_β . Whereas $D(i\omega_0)$ of f_α monotonically increases upon cooling (see inset of Fig. 3 (b)), $D(i\omega_0)$ of f_β is nearly temperature-independent between 150 K and 300 K. It exhibits a local minimum at 50 K before sharply increasing at lower temperatures. We attribute our observations to the Kondo scattering involving f_β and $\text{Te}2-p_{\{3,6\}}$ at $T = 50$ K (see Fig. S3 (b)). We thus define $T_{\text{KS}}^{p\pm} = 50$ K as the onset temperature of the Kondo effect along the c -axis, and, χ_{charge} of f_β manifests a sudden drop below $T = 30$ K as shown in Fig. 3 (c). The hybridization between f_β and $\text{Te}2-p_{\{3,6\}}$ is responsible for the c -axis transport, and our result is consistent with the recent experiment where ρ_c is metallic in $\sim 50 \text{ K} < T < 300 \text{ K}$ and exhibits an upturn below $\sim 50 \text{ K}$ [1] as shown in Fig. 3 (f).

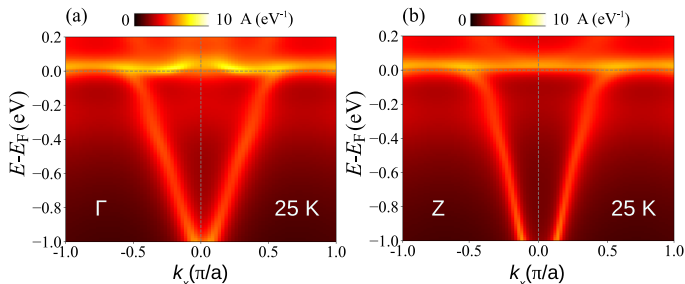


FIG. 4. Momentum-resolved total spectral function along the (a) Γ -X and (b) X_1 -Z- X_1 . The simulation temperature is 25 K for both.

ARPES- We compare our calculated spectral function at $T = 25$ K to recent ARPES measurements at $T = 20$ K [16, 17]. The calculated spectral functions along the Γ -X and Z- X_1 consist of one parabolic band and incoherent spectral weights, which agree with both measured ARPES spectra in the binding energy of $E_B < 1.0$ eV along the same symmetry lines. Particularly, dispersive Kondo resonance peaks near the Fermi level (which is not presented in the non-SOC spectral function.) appear in the ARPES [16]. There are incoherent f_β bands in $-0.2 \text{ eV} > E - E_F > -0.4 \text{ eV}$. The corresponding bands appear in $-0.4 \text{ eV} > E - E_F > -0.6 \text{ eV}$ in both ARPES data. As shown in Fig. 3 (d), the spectral weight is more pronounced at lower energy down to 25 K from 300 K. Also, transport measurement shows abrupt change on the resistivity below 50 K (see Fig. 3 (f)), indicating the rapid change on the electronic structure. Thus, we suggest that the

variance may partly be caused by the temperature difference between simulation and ARPES measurement.

Summary - We performed first-principles simulations to investigate the electronic structure of heavy-fermion superconductor UTe_2 . We found that the inclusion of SOC is necessary to reproduce the observed occupancy of the $5f$ orbital-configuration, anomalous temperature-dependence of electrical resistivity by Kondo effect, and band structure near the Fermi level measured by ARPES. In regard to electron correlations in heavy-fermion compounds, we note a number of DFT+DMFT studies for Ce- and Pu-based compounds [15, 19, 20, 24, 46], where conduction electron (d or p) dependent correlations is not found. As such, our discovery suggests that UTe_2 has complex electronic structure, which manifests unprecedented orbital-selective hybridization among $f_{\{1,6\}}$, $f_{\{2,3,4,5\}}$, d , and p orbitals. Our description of rich physics of the normal state in UTe_2 may provide key knowledge for the understanding of unconventional superconductivity.

Acknowledgements - The authors would like to thank Yun Suk Eo and Johnpierre Paglione for sharing the electrical transport data and insightful discussion. We acknowledge the High Performance Computing Center (HPCC) at Texas Tech University for providing computational resources that have contributed to the research results reported within this paper. S.C. was supported by the U.S. Department of Energy, Office of Science, Basic Energy Sciences as a part of the Computational Materials Science Program. Coulomb interaction tensor calculation used resources of the National Energy Research Scientific Computing Center (NERSC), a U.S. Department of Energy Office of Science User Facility operated under Contract No. DE-AC02-05CH11231

* byungkyun.kang@unlv.edu

† hyunsoo.kim@ttu.edu

- [1] Y. S. Eo, S. R. Saha, H. Kim, S. Ran, J. A. Horn, H. Hodovanets, J. Collini, W. T. Fuhrman, A. H. Nevidomskyy, N. P. Butch, M. S. Fuhrer, and J. Paglione, arXiv:2101.03102 (2021).
- [2] D. Aoki, K. Ishida, and J. Flouquet, *Journal of the Physical Society of Japan* **88**, 022001 (2019).
- [3] D. Aoki, A. Huxley, E. Ressouche, D. Braithwaite, J. Flouquet, J.-P. Brison, E. Lhotel, and C. Paulsen, *Nature* **413**, 613 (2001).
- [4] N. T. Huy, A. Gasparini, D. E. de Nijs, Y. Huang, J. C. P. Klaasse, T. Gortenmulder, A. de Visser, A. Hamann, T. Görlach, and H. v. Löhneysen, *Phys. Rev. Lett.* **99**, 067006 (2007).
- [5] S. Ran, C. Eckberg, Q.-P. Ding, Y. Furukawa, T. Metz, S. R. Saha, I.-L. Liu, M. Zic, H. Kim, J. Paglione, and N. P. Butch, *Science* **365**, 684 (2019).
- [6] P. F. S. Rosa, A. Weiland, S. S. Fender, B. L. Scott, F. Ronning, J. D. Thompson, E. D. Bauer, and S. M. Thomas, arXiv:2110.06200 (2021).
- [7] D. Aoki, J. P. Brison, J. Flouquet, K. Ishida, G. Knebel, Y. Tokunaga, and Y. Yanase, arXiv:2110.10451 (2021).
- [8] S. Ran, H. Kim, I.-L. Liu, S. R. Saha, I. Hayes, T. Metz, Y. S. Eo, J. Paglione, and N. P. Butch, *Phys. Rev. B* **101**, 140503 (2020).

- [9] W. Knafo, M. Nardone, M. Vališka, A. Zitouni, G. Lapertot, D. Aoki, G. Knebel, and D. Braithwaite, *Communications Physics* **4**, 40 (2021).
- [10] D. Aoki, A. Nakamura, F. Honda, D. Li, Y. Homma, Y. Shimizu, Y. J. Sato, G. Knebel, J.-P. Brison, A. Pourret, *et al.*, *Journal of the Physical Society of Japan* **88**, 043702 (2019).
- [11] O. Trovarelli, C. Geibel, S. Mederle, C. Langhammer, F. M. Grosche, P. Gegenwart, M. Lang, G. Sparn, and F. Steglich, *Phys. Rev. Lett.* **85**, 626 (2000).
- [12] C. Petrovic, P. G. Pagliuso, M. F. Hundley, R. Movshovich, J. L. Sarrao, J. D. Thompson, Z. Fisk, and P. Monthoux, *Journal of Physics: Condensed Matter* **13**, L337 (2001).
- [13] P. Aynajian, E. H. da Silva Neto, A. Gyenis, R. E. Baumach, J. D. Thompson, Z. Fisk, E. D. Bauer, and A. Yazdani, *Nature* **486**, 201 (2012).
- [14] Q. Y. Chen, D. F. Xu, X. H. Niu, J. Jiang, R. Peng, H. C. Xu, C. H. P. Wen, Z. F. Ding, K. Huang, L. Shu, Y. J. Zhang, H. Lee, V. N. Strocov, M. Shi, F. Bisti, T. Schmitt, Y. B. Huang, P. Dudin, X. C. Lai, S. Kirchner, H. Q. Yuan, and D. L. Feng, *Phys. Rev. B* **96**, 045107 (2017).
- [15] S. Jang, J. D. Denlinger, J. W. Allen, V. S. Zapf, M. B. Maple, J. N. Kim, B. G. Jang, and J. H. Shim, *Proceedings of the National Academy of Sciences* **117**, 23467 (2020).
- [16] S.-i. Fujimori, I. Kawasaki, Y. Takeda, H. Yamagami, A. Nakamura, Y. Homma, and D. Aoki, *Journal of the Physical Society of Japan* **88**, 103701 (2019).
- [17] L. Miao, S. Liu, Y. Xu, E. C. Kotta, C.-J. Kang, S. Ran, J. Paglione, G. Kotliar, N. P. Butch, J. D. Denlinger, and L. A. Wray, *Phys. Rev. Lett.* **124**, 076401 (2020).
- [18] J. Kondo, *Progress of Theoretical Physics* **32**, 37 (1964).
- [19] H. C. Choi, K. Haule, G. Kotliar, B. I. Min, and J. H. Shim, *Phys. Rev. B* **88**, 125111 (2013).
- [20] H. C. Choi, B. I. Min, J. H. Shim, K. Haule, and G. Kotliar, *Phys. Rev. Lett.* **108**, 016402 (2012).
- [21] H. Lu and L. Huang, *Phys. Rev. B* **94**, 075132 (2016).
- [22] J. Kim, D.-C. Ryu, C.-J. Kang, K. Kim, H. Choi, T.-S. Nam, and B. I. Min, *Phys. Rev. B* **100**, 195138 (2019).
- [23] X.-G. Zhu, Y. Liu, Y.-W. Zhao, Y.-C. Wang, Y. Zhang, C. Lu, Y. Duan, D.-H. Xie, W. Feng, D. Jian, Y.-H. Wang, S.-Y. Tan, Q. Liu, W. Zhang, Y. Liu, L.-Z. Luo, X.-B. Luo, Q.-Y. Chen, H.-F. Song, and X.-C. Lai, *npj Quantum Materials* **5**, 47 (2020).
- [24] W. H. Brito, S. Choi, Y. X. Yao, and G. Kotliar, *Phys. Rev. B* **98**, 035143 (2018).
- [25] M. Zarea, S. E. Ulloa, and N. Sandler, *Phys. Rev. Lett.* **108**, 046601 (2012).
- [26] Y. Xu, Y. Sheng, and Y.-f. Yang, *Phys. Rev. Lett.* **123**, 217002 (2019).
- [27] J. M. Tomczak, in *Journal of Physics: Conference Series*, Vol. 592 (IOP Publishing, 2015) p. 012055.
- [28] S. Choi, A. Kutepov, K. Haule, M. van Schilfhaarde, and G. Kotliar, *npj Quantum Materials* **1**, 16001 (2016).
- [29] S. Choi, P. Semon, B. Kang, A. Kutepov, and G. Kotliar, *Computer Physics Communications* **244**, 277 (2019).
- [30] K. Stöwe, *Journal of Solid State Chemistry* **127**, 202 (1996).
- [31] S. Ikeda, H. Sakai, D. Aoki, Y. Homma, E. Yamamoto, A. Nakamura, Y. Shiokawa, Y. Haga, and Y. Ōnuki, *Journal of the Physical Society of Japan* **75**, 116 (2006).
- [32] P. Sun and G. Kotliar, *Phys. Rev. B* **66**, 085120 (2002).
- [33] S. Biermann, F. Aryasetiawan, and A. Georges, *Phys. Rev. Lett.* **90**, 086402 (2003).
- [34] F. Nilsson, L. Boehnke, P. Werner, and F. Aryasetiawan, *Phys. Rev. Materials* **1**, 043803 (2017).
- [35] A. Kutepov, K. Haule, S. Y. Savrasov, and G. Kotliar, *Phys. Rev. B* **85**, 155129 (2012).
- [36] A. Kutepov, V. Oudovenko, and G. Kotliar, *Computer Physics Communications* **219**, 407 (2017).
- [37] A. Georges, G. Kotliar, W. Krauth, and M. J. Rozenberg, *Rev. Mod. Phys.* **68**, 13 (1996).
- [38] W. Metzner and D. Vollhardt, *Phys. Rev. Lett.* **62**, 324 (1989).
- [39] A. Georges and G. Kotliar, *Phys. Rev. B* **45**, 6479 (1992).
- [40] F. Aryasetiawan, M. Imada, A. Georges, G. Kotliar, S. Biermann, and A. I. Lichtenstein, *Phys. Rev. B* **70**, 195104 (2004).
- [41] See Supplemental Material for details.
- [42] K. Stöwe, *Journal of Alloys and Compounds* **246**, 111 (1997).
- [43] X. Deng, K. M. Stadler, K. Haule, A. Weichselbaum, J. von Delft, and G. Kotliar, *Nature Communications* **10**, 2721 (2019).
- [44] W. Koller, A. C. Hewson, and D. Meyer, *Phys. Rev. B* **72**, 045117 (2005).
- [45] A. Koga, N. Kawakami, T. M. Rice, and M. Sigrist, *Phys. Rev. B* **72**, 045128 (2005).
- [46] H. Lu and L. Huang, *Phys. Rev. B* **103**, 205134 (2021).